SST-driven variability of the East Asian summer jet on a decadal time-scale in CMIP6 models

Article

Accepted Version

CentAUR

Central Archive at the University of Reading

Reading's research outputs online

SST-driven variability of the East Asian summer jet on a decadal timescale in CMIP6 models

Matthew Patterson[1*] | Christopher O'Reilly[2†] | Tim Woollings[1†] | Antje Weisheimer[1,3,4†] | Bo Wu[5†]

[1]Atmospheric, Oceanic and Planetary Physics, University of Oxford, United Kingdom

[2]University of Reading, United Kingdom

[3]National Centre for Atmospheric Science, University of Oxford, United Kingdom

[4]European Centre for Medium-Range Weather Forecasts, United Kingdom

[5]State Key Laboratory of Numerical Modeling for Atmospheric Sciences and Geophysical Fluid Dynamics, Institute of Atmospheric Physics, Chinese Academy of Sciences, and Joint Center for Global Change Studies, China

Correspondence
Matthew Patterson, Atmospheric, Oceanic and Planetary Physics, University of Oxford, United Kingdom
Email: matthew.patterson@physics.ox.ac.uk

The East Asian summer jet (EASJ) is an important component of the East Asian summer monsoon system and its variability is correlated with precipitation and surface temperature variations over this region. Whilst many studies have considered the interannual variability of the EASJ, less is known about variations on a decadal timescale. This study investigates the relationship between decadal EASJ variability and sea surface temperatures (SSTs) and thus the potential predictability that SSTs may provide. Given the relatively short observational record, we make use of the long preindustrial control simulations in the Coupled Model Intercomparison Project phase 6 (CMIP6) in addition to a large ensemble of atmosphere-only experiments, forced with random SST patterns. We then create an SST-based reconstruction of the dominant modes of EASJ variability in the CMIP6 models, finding a median EASJ-reconstruction correlation for the dominant mode of 0.43. Much of the skill in the reconstruction arises from variations in Pacific SSTs, however the tropical Atlantic also makes a significant contribution. These findings suggest the potential for multi-year predictions of the EASJ, provided that skillful SST forecasts are available.

KEYWORDS

[*]Equally contributing authors.

1 | INTRODUCTION

From the mid twentieth century to the present day, East Asian summer climate has been subject to considerable interdecadal variability. This has included a weakening of the East Asian summer monsoon system, particularly around the late 1970s [1, 2, 3], with a concomitant southward shift of the East Asian jet [4]. These atmospheric circulation changes are reflected in the precipitation record including enhanced rainfall over the Yangtze river valley in southern China and reductions over northern China [5, 3], a pattern referred to as Southern Flood Northern Drought. A further change in precipitation patterns occurred around the early 1990s with intensified precipitation to the south of the Yangtze river [6, 7].

Given the high impact of these climatic changes on society, a number of studies have sought to understand to what extent they can be explained through natural and anthropogenically forced variability, though no clear consensus has yet emerged. Models forced with observed sea surface temperatures (SSTs) have been shown to largely reproduce observed changes to the East Asian summer monsoon [8, 9]. Some studies have concluded that anthropogenic aerosols play a key role in the monsoon weakening [10, 11, 12, 13, 14], however others have argued for the importance of greenhouse gas-induced changes [15, 16]. Tian et al. [17] found that both forcings play a role, but in different regions as aerosol forcing dominates precipitation anomalies over northern China while greenhouse gas forcing is most important for southern regions. Other studies have also emphasised that natural variability may be a substantial factor [18, 7, 19].

The focus of this study is the East Asian summer jet (EASJ), an important component of the East Asian summer monsoon system. Variability of the EASJ is predominantly characterised by a meridonal shifting of the jet and this is strongly correlated with precipitation anomalies in observations [20, 21, 22, 23, 24]. However, this relationship has been found to be too weak in models [25], possibly due to biases in the climatological jet [26] or tropical rainfall [27]. Interannual variations in the EASJ have been linked to tropical Indian Ocean SST variability [28], central Pacific SST anomalies [23] and surface temperatures over the Russian far-east [29]. On longer timescales, Song et al. [13] argued that the observed southward jet shift at the end of the twentieth century can be explained via a combination of aerosol forcing and natural variability. On the other hand, there has been little work on the specific teleconnections and mechanisms underlying natural decadal EASJ variability. It is possible that mechanisms which modulate jet variability on interannual timescales also operate on decadal timescales, for instance decadal variability of the Indian Ocean could affect the jet via the Pacific-Japan pattern [30]. Additionally, the Pacific Decadal Oscillation (PDO) and Atlantic Multi-decadal Variability (AMV) have both been suggested as drivers of precipitation over East Asia in observational studies and these may also drive EASJ variability [31, 32].

Observational studies of jet variability on decadal timescales typically encounter two main challenges. Firstly, they are hampered by the relatively short time series' of available reanalysis datasets which stretch back at most around 120 years. PDO and AMV anomalies can persist for 20-30 years in the observational record and hence the associated number of degrees of freedom is very low. Furthermore, upper tropospheric atmospheric circulation is relatively unconstrained in long reanalysis datasets which assimilate only sea level pressure, surface winds and sea surface temperatures, rendering earlier time periods less reliable. Secondly, disentangling the physical mechanisms which are responsible for climate variations is also difficult because of the presence of anthropogenic aerosols and direct greenhouse gas forcing. Consequently, in this study we make use of the long pre-industrial control (piControl) runs performed by modelling centres participating in the Coupled Model Intercomparison Project phase 6 [CMIP6,

33]. These coupled simulations are typically around 500 years in length, with no externally forced variability. The use of coupled simulations also allows for the interaction between ocean and atmosphere which is not present in simulations forced with prescribed SSTs.

In this study, we specifically seek to address three main questions:

1. What is the nature of variability of the EASJ on a decadal timescale and how does this variability affect the surface climate?
2. To what extent is this variability predictable based on SST forcing?
3. What are the mechanisms by which SST - EASJ teleconnections occur?

The rest of this paper is structured as follows. The data and methods are described in section 2 with an analysis of decadal jet variability in the CMIP6 models following in section 3. Section 4 quantifies the strength of SST-EASJ covariability across models, while section 5 seeks to further understand the mechanisms behind these teleconnections. A brief examination of inter-model differences is given in section 6 and finally, a discussion of the results and conclusions are given in section 7.

2 | DATA AND METHODS

2.1 | CMIP6 pre-industrial control (piControl) data

In this study we make use of data from the long piControl runs available from 28 climate models in the CMIP6 archive. These are free-running, coupled simulations, typically of around 500 years in length, though some span up to 1200 years. There is no forced interannual variability in these models due to, for example, volcanic eruptions or insolation, while orbital parameters and greenhouse gas concentrations are fixed at their approximate level in the year 1850 [33]. From this set of model runs, we utilize seasonal mean data for the summer season (June, July, August - JJA). A full list of the models along with the number of years in each simulation, can be found in the supplementary material.

2.2 | Atmosphere-only experiments

We also analyse an ensemble of 5000 atmosphere-only model runs forced with randomly perturbed SSTs from the study of Baker et al. [34], following the method of Li et al. [35] and Li and Forest [36]. These simulations provide a useful comparison to coupled simulations, as the SSTs can only force the atmosphere and not vice-versa, making the direction of causality clear. On the other hand, there are many regions of the real world in which SSTs are strongly forced by atmospheric variability on interannual and longer timescales and hence the model will not represent atmosphere-ocean coupling correctly in these regions. SST perturbations are constructed by creating a 16 x 16 grid and drawing a value from a uniform distribution at each point between -2K and 2K. This grid is then interpolated onto the full model grid and the perturbation field is randomly shifted by up to 8 grid-points in latitude and up to 5 in the meridional direction. Following this the perturbation field is added to the monthly varying climatology of SSTs, calculated using the merged Hadley–NOAA optimum interpolation (OI) SST dataset for the period 1980-1999. The perturbations are only applied between 60S and 60N. The model runs are performed using the Met Office HadAM3P model which has a resolution of 1.875 x 1.25 in the horizontal and 19 hybrid sigma levels in the vertical. Each ensemble member is run out to 25 months beginning in December, while in our analysis we only investigate the second summer (JJA).

2.3 | Reanalyses

The Met Office Hadley Centre's sea ice and sea surface temperature data set (HadISST) version 2.1.0.0 [37] is used for the analysis of SSTs. Seasonal mean data from three atmospheric reanalyses datasets covering different time periods are also used. These are ERA20C [38], JRA-55 [39] and NCEP/NCAR [40], which span the periods 1900-2010, 1958-present and 1948-present, respectively.

2.4 | Jet indices

We calculate indices of EASJ variability using Empirical Orthogonal Function (EOF) analysis. We define indices as the principal component time series associated with the leading two EOFs 200hPa zonal wind within the East Asian region, which we define by longitudes 70-150E and latitudes 20-50N (shown by a box in figure 2). The jet EOF patterns are not particularly sensitive to variations of order $10°$ in any direction. Following this, a low pass filter is applied to the EASJ EOF indices to extract only the multi-year / decadal signal, apart from in figures 1a-d) and 6a) and those involving the atmosphere-only model, where the interannual variability is retained. The low pass filter consists of a 7 year running mean applied at all grid-points and the EOF analysis is performed using the Python package, 'eofs' [41].

2.5 | Linear sensitivity analysis

Data from the atmosphere-only runs can be utilized to calculate the linear sensitivities of the EASJ to SST forcing. Following Li et al. [35], under the assumption of a linear response (ΔR) to SST anomalies (ΔSST), the response is given by

$$\Delta R = \int_{A'} G(x')\Delta SST(x')dA' + e, \tag{1}$$

where x' is the spatial co-ordinate, $G(x')$ is a linear operator (or Green's function), A' is the area integrated over x' and e is the associated error due to non-linearities and internal variability. $G(x')$ gives the linear sensitivity of the response to SST perturbations at a particular location. In our case, ΔR is the EASJ index response to SST forcing. Given that the model is discrete, we calculate G at each grid-point using the linear regression model

$$\Delta R = G\Delta SST + e. \tag{2}$$

Following this, the estimated response of the EASJ index can be reconstructed for any given pattern of SST anomalies via

$$\Delta R = \gamma \sum_{\mathbf{x_i}} G(\mathbf{x_i})\Delta SST(\mathbf{x_i})L_x L_y, \tag{3}$$

where γ is a constant which depends on the length scale of the forcing [see 35], $\mathbf{x_i}$ is a vector of grid-points and ΔSST is the SST anomaly field. $L_x = a\lambda_0 cos\phi_i$ and $L_y = a\phi_0$ are the zonal and meridional length scales, a is the radius of the Earth, ϕ_i is the latitude, while ϕ_0 and λ_0 are the meridional and zonal grid-point spacings in radians, respectively.

In our study, we calculate G using the atmosphere-only runs and use it to attempt to reconstruct EASJ variability in the CMIP6 models, using only SST anomalies. In doing so, this will allow us to quantify the extent to which SST anomalies alone can explain EASJ variability. There are a number of limitations to this analysis. Firstly, we assume that SST anomalies combine linearly to produce the given response, though this appears to be a good assumption in the case of the EASJ (see supplementary figures S1 and S2). Secondly, prescribing SSTs in the atmosphere-only model means that the SSTs are unable to respond to atmospheric perturbations. Thirdly, atmospheric circulation anomalies may correlate with local SSTs in the real world because of reduced thermal damping which does not enhance predictability [42]. Finally, the atmosphere-only runs are relatively short at only 25 months in comparison to the decadal timescales in which we are interested. However, we may assume that any long term memory in the system persists through the ocean component of the system and that the atmosphere responds relatively quickly (on a timescale of months) to given SST anomalies. In spite of these limitations, this method has previously proven skillful in predicting tropospheric geopotential height variability over the Pacific [43] and jet variability in the North Atlantic [34].

2.6 | Significance tests

Given that we are considering long timescale variability, many of the time series under investigation exhibit serial correlation, reducing the effective size of the sample. Consequently, we employ the method of Ebisuzaki [44] to calculate a threshold correlation for statistical significance at the 95% level. Considering two time series, A and B, the procedure begins by finding the discrete Fourier transform of A and generating 1000 surrogate time series through multiplication of the Fourier components by a set of random phases, before performing the inverse Fourier transform. That is, the Fourier components, a_m are each multiplied by $e^{i\theta_m}$, where θ_m are drawn from a uniform distribution between 0 and 2π. Following this, a distribution is created by calculating correlations between B and the surrogate time series', and the correlation between A and B is deemed to be significant if it is larger in magnitude than 95% of the correlations in this distribution.

3 | DECADAL EASJ VARIABILITY AND ITS IMPACT ON SURFACE CLIMATE

We begin by examining the dominant patterns of decadal jet variability over East Asia and associated patterns of surface climate variability in CMIP6 piControl runs. Figure 1a,b) shows the observed 200hPa zonal wind patterns associated with interannual variability of the EASJ EOF indices, calculated using JRA-55 reanalysis data. EASJ EOF 1 is characterised by a meridional shifting of the EASJ, while EASJ EOF 2 is associated with a strengthening / weakening jet, in agreement with other studies [e.g. 28]. Figure 1c,d) shows that these patterns are well reproduced by the CMIP6 models, though in a few models ('CNRM-CM6-1', 'CNRM-ESM2-1' and 'MIROC6') the first two EOFs are not statistically well separated using the method of North et al. [45, not shown]. Overall the EASJ EOFs 1 and 2 explain around 30-35% and 20-25% of the variance in most models, respectively (figure 1g). We are primarily interested in multi-year variability of the EASJ, hence we apply a 7 year running mean to the model EASJ EOF indices to extract the low frequency component of EASJ variability. We regress these decadal EASJ EOF indices onto 200hPa zonal wind, which has been similarly low-pass filtered at each grid-point, in figure 1e,f). The associated patterns are very similar to their interannual equivalents (figure 1c,d). Note that very similar patterns are obtained if the 200hPa zonal wind data is low-pass filtered before the EOFs are calculated (not shown).

We next regress these decadal EASJ EOF indices onto some variables describing surface climate variability. Comparing figure 2a) with figure 1e), upper level EASJ variability exhibits a largely baroclinic structure as the poleward

shifted EASJ (EOF 1) is associated with a surface high over southern Japan, and hence anomalous low-level, westerly flow at around 40N (figure 2a), with a poleward low. EASJ EOF 2 is also baroclinic, as strengthening of the jet is linked to a sea level pressure dipole consisting of a low over most of Japan and a high to its south (figure 2d). There is a strong surface temperature signature linked to EASJ variability. Poleward shifts of the EASJ are correlated with warm anomalies over most of China and Japan, with the latter showing multi-model mean correlations in excess of 0.5 over much of the country 2c). Unlike in observations, EASJ variability is not strongly correlated with precipitation anomalies in the CMIP6 models, at least in the ensemble-mean (figure 2e,f). This is in agreement with previous literature, which mostly examined CMIP5 models [25, 26, 27]. The low correlations in the multi-model mean may partly be a consequence of the fact that precipitation is a noisy variable and varies considerably over small spatial scales, hence subtle variations in mean jet position could have large effects on precipitation correlation maps. Examining similar plots to figure 2e,f), but for individual models, precipitation correlation values over China can be in excess of 0.5 (not shown).

4 | SST-BASED PREDICTABILITY OF EASJ VARIABILITY

To investigate the connection between SSTs and decadal EASJ variability, we calculate correlations between the jet EOF indices and SSTs for each model, with SSTs low-pass filtered at each grid-point. Figure 3a,b) shows the multi-model mean correlations for EOFs 1 and 2, indicating that a poleward shift of the jet is negatively correlated with SSTs in the western Indian Ocean, tropical Pacific and tropical Atlantic, with a region of positive correlations to the east of Japan. Conversely, the strengthening / weakening jet mode is not linked to tropical SST variations, but only local SST anomalies. Interestingly, the multi-model mean masks a wide variation in the magnitude of SST-EASJ correlation strength across models. For instance, some models such as CNRM-CM6-1-HR show no significant correlation with tropical SST at all (figure 3c,d), whereas others such as HadGEM3-GC31-LL, show correlation values of −0.6 at some locations. Generally speaking, the EASJ EOF 1 correlation maps resemble the negative phase of the PDO (figure 3a,c,e) over the Pacific. It is also worth noting that the PDO is defined by extratropical North Pacific SSTs and the magnitude of PDO projection onto the tropics varies considerably between models [46], which may be related to the inter-model differences in SST-EASJ correlations.

On the other hand, the negative correlations of EOF 1 with tropical Atlantic and Indian Ocean SSTs suggest that variability in these regions may also be important. To investigate the role of different SST anomalies in forcing EASJ variability, we calculate the linear sensitivity operator, G, as described in section 2. Firstly, it is important that EASJ variability in the atmosphere-only model is similar to that in the coupled models. Hence, we plot regressions of the principal component time series associated with EOFs 1 and 2 in HadAM3P onto 200hPa zonal wind anomalies in figure 4. The first two EOFs explain a similar amount of variance to the coupled model EOFs at 32% and 22% for EOFs 1 and 2 respectively. Furthermore, as for the CMIP6 models, EOF 1 manifests as a shifting of the EASJ, while EOF 2 is characterised by strengthening / weakening of the EASJ (figure 1c-f). Therefore, we conclude that the jet variability in HadAM3P is sufficiently similar to CMIP6 for our analysis.

The sensitivity patterns, G, for the different EASJ EOF indices are shown in figure 5. Similar to figure 3a), negative SST anomalies in the tropics are generally associated with a poleward shift of the jet (i.e. positive EOF 1, figure 5a). Interestingly, EOF 1 shows a particularly strong sensitivity to tropical Indian Ocean cooling between 10S and 10N, however, EOF 1 is also associated with opposite signed SST anomalies over northern parts of the Indian Ocean. There is also a region of sensitivity to warm SSTs over the North-West Pacific, stretching northward to the climatological jet latitude. With regard to EOF 2 (strengthening / weakening), the strongest sensitivity is again the North-West Pacific

region, however it is worth noting that observed SST variability in this region is primarily forced by atmospheric anomalies [47]. Positive EOF 2 is also sensitive to warm anomalies over the tropical Pacific and Atlantic.

Given the sensitivity patterns, we can attempt to reconstruct the EASJ jet indices by projecting SST anomalies for each year onto the sensitivity patterns using equation 3, and comparing the resulting index to the true EASJ indices. The interannual variability of EASJ EOF 1 is shown for three reanalysis datasets in figure 6a). In general these three indices are in relative agreement with each other with correlation values during overlapping periods as follows: $R(\text{NCEP, ERA-20C}) = 0.77$, $R(\text{NCEP, JRA-55}) = 0.84$ and $R(\text{JRA-55, ERA-20C}) = 0.82$. The SST-based reconstruction of EASJ EOF 1 is also plotted in red and is significantly positively correlated with all three reanalyses. However, the focus of the present study is decadal variability, hence we apply a 7 year running mean to these time series and plot this in figure 6b). The longest time series, ERA-20C, bears little resemblance to the SST-based reconstruction on these longer time scales and is not significantly correlated. This may be partly because ERA-20C assimilates only surface observations and hence upper level jet variability is poorly constrained. Conversely, both NCEP/NCAR and JRA-55 are strongly positively correlated with the EASJ reconstruction, at $R = 0.68$ and $R = 0.72$ respectively, though with the caveat of severely limited sample sizes. Given this limitation, we cannot draw firm conclusions from these reconstructions, but the strong correlations of the shorter reanalyses suggest that SSTs may provide some skill in predicting jet variability. Furthermore, the reconstructions are skillful on interannual timescales which provides us with confidence in the performance of the atmosphere-only model and suggests that SSTs do indeed influence the jet in observations. Interestingly the Pacific region makes up by far the largest component of the decadal jet reconstruction (figure 6c) suggesting that the Pacific is the most important source of skill in this reconstruction. In contrast to EOF 1, SST-based reconstructions of EOF 2 are not significantly correlated with EOF 2 in reanalysis (not shown) despite the extensive regions of significant sensitivity shown in figure 5b).

We can study longer time series by applying the same methodology to the CMIP6 piControl runs. Furthermore, the linearity of the SST-sensitivity approach means that it is straightforward to attribute SST prediction skill to SST anomalies in different regions by only projecting SST anomalies onto the sensitivity pattern in certain regions. An example of this is shown for the CESM2 model, with a low pass filter applied as in figure 6b) for the projection onto the entire sensitivity pattern and for different longitudinal bands in figure 7. The regions are defined by the longitudes 120E-80W, 80W-30E and 30E-120E, for the Pacific, Atlantic and Indian Ocean regions respectively. In comparison to the reanalyses, the CESM2 simulation is far longer and hence does not suffer from the same sampling issues. The global reconstruction has a correlation coefficient of 0.4, while the Pacific on its own has a correlation coefficient of 0.42, suggesting that this region provides the majority of the reconstruction skill. The Atlantic SST- EASJ reconstruction is also significantly correlated with EASJ EOF 1, however the Indian Ocean region is not.

Next, we apply this procedure to all CMIP6 piControl runs and create box plots of the resulting EASJ reconstruction correlations, shown in figure 8. The length of the piControl runs varies between models, hence the 95% significance threshold will also vary. Given that all model runs are 500 years or longer, we plot the significance threshold calculated for a model run of this length (dashed line in figure 8). Similar to CESM2 in figure 7, the majority of models have an EASJ EOF 1 reconstruction correlation close to 0.4, with quartiles of 0.34 to 0.46, and almost all models show a significant reconstruction correlation (figure 8a). Once again, the Pacific appears to explain the majority of the skill and the Atlantic is also significantly positively correlated, while the Indian Ocean SST reconstruction is not. The lack of Indian Ocean skill is interesting given the strong sensitivity values in this region (figure 5a). It is possible that circulation anomalies from other decadal timescale patterns such as the PDO dominate any atmospheric variability forced by the Indian Ocean.

In section 2, we noted that one limitation of this analysis is that atmospheric circulation anomalies may arise due to thermal damping of local SSTs, a process which doesn't provide any additional predictability [42]. The Pacific

sensitivity pattern projects onto a region of SSTs close to the jet itself (figure 5a), hence it is also useful to repeat the SST reconstruction analysis including only the tropics, as regions far from the jet will not suffer from this issue. The results of the tropics-only analysis are shown in figure 8a) by blue boxplots. Removing the extratropical SST projection reduces the median global correlation strength slightly to 0.3 and also broadens the range of correlation values, although global correlations in most models remain significant. A similar picture is seen for the Pacific-only case, confirming that the sensitivity region east of Japan contributes to the jet correlation skill, but also that significant skill remains when this region is excluded. For completeness, we also show EASJ reconstruction correlations for EOF 2 in figure 5b). Similar to EOF 1, the SST-based reconstruction has some skill in reproducing EASJ variability, however, this skill is largely absent for the tropics-only model reconstructions. This is consistent with figure 3b) in which only local, extratropical SSTs are correlated with EASJ EOF 2 variability across models. It is also woth noting that using the piControl models themselves to calculate the sensitivity patterns gives similar results to using the atmosphere-only model (figure S3, supplementary material), increasing confidence in the method.

5 | SST-EASJ TELECONNECTION MECHANISMS

Given that it is possible to partially reconstruct decadal EASJ variability based solely on SSTs, we now investigate the mechanisms underlying SST-EASJ covariability. We initially consider the mechanisms present in the atmosphere-only runs and then compare these to the piControl simulations. We define SST indices for three different regions, namely the Indian Ocean, tropical Pacific and tropical Atlantic. The Indian Ocean is defined as 10S-10N, 40E-110E; tropical Pacific is defined as the Nino3.4 region, 5S-5N, 170W-120W; and the tropical Atlantic by SST 10S-20N, 80W-0E. Note that the SST indices have each been standardised, hence the use of different sizes of areas does give slightly different magnitudes of SST anomalies in figure 9a,c,e).

Figure 9 shows regressions of the mean SST anomalies within these boxes onto SST, precipitation, sea level pressure and 200hPa zonal wind anomalies. We consider the Indian Ocean first as although this does not provide significant skill to the EASJ reconstructions, it is a region of considerable sensitivity in the atmosphere-only runs (figure 5a). In this region, warm SST anomalies are associated with negative sea level pressure anomalies, positive precipitation anomalies (i.e. anomalous convection) and diverging upper level zonal wind (figure 9d,g,j). The presence of the North-West Pacific anticyclonic anomaly (figure 9b) is consistent with the Indian Ocean capacitor mechanism [30, 48], whereby a tropospheric Kelvin wave, initiated by convection over the Indian Ocean, induces subsidence, boundary layer divergence and suppressed convection over the Philippines. This process maintains a low level subtropical high over the Philippines (figure 9g). This shifts the EASJ southward (figure 9g), consistent with the findings of Qu and Huang [28].

Warm Pacific SSTs are also associated with negative sea level pressure anomalies and anomalous convection (figure 9e,h). Regarding the mechanism for the teleconnection to the EASJ, this appears to be consistent with the strengthening and equatorward shift of the subtropical jet under an El Niño-like warming pattern [49, 50]. That is, tropical SSTs warm the tropical troposphere (not shown), which enhances the meridional temperature gradient between the tropics and subtropics, strengthening and shifting the subtropical jet through thermal-wind balance. Lastly, the local atmospheric response to Atlantic SSTs is again characterised by low sea level pressure and enhanced precipitation (figure 9f,i). This induces positive sea level pressure anomalies over the Pacific, including a strengthened North-West Pacific subtropical high (figure 9i). Rong et al. [51] found a similar result using both observations and model experiments and argued that enhanced convection over the tropical Atlantic drives an atmospheric Kelvin wave which propagates eastwards affecting both the Indian and East Asian monsoon systems. Similar to the Indian

Ocean and tropical Pacific indices, tropical Atlantic SSTs are linked to positive zonal wind anomalies to the south of Japan and hence an equatorward shift of the EASJ (figure 9l). To summarise, when warm SSTs are imposed in the tropics in the atmosphere-only runs, the local response is consistent with deep ascent in each case, as expected from basic theory [e.g. 52]. These local responses then each generate cause an upper level response which modulates the EASJ.

The EASJ reconstructions assume that the teleconnection mechanisms in the atmosphere-only runs are replicated in the piControl simulations on decadal timescales, hence we test this by defining SST indices in the piControl runs, using the same regions. This time, the SSTs are low pass filtered when defining the indices to extract only the decadal variability. Given that there is large covariability between the different ocean basins, particularly on decadal timescales, we also regress the tropical Pacific index out from the Indian Ocean and tropical Atlantic indices to isolate the impact that SSTs in the Indian Ocean and tropical Atlantic have. That is, variability associated with the tropical Pacific is removed from the other two indices so that the tropical Pacific and Indian Ocean / tropical Atlantic indices are uncorrelated. Each index is standardised before removing the variability associated with the tropical Pacific.

Indian Ocean SSTs do not add skill to the reconstructions of the EASJ in most models (figure 8), in spite of the EASJ sensitivity to SSTs in this region in the atmosphere-only runs (figure 5a). Two possible hypotheses for this result are 1), that the atmosphere-only runs capture a teleconnection which is not present in the coupled models and 2), the teleconnection exists but explains little of the EASJ variance due to dominance of other forcings or internal EASJ variability. Figure 10 suggests that the former explanation is unlikely. It shows a composite of the seven models with the largest EASJ-SST covariability, in which the SST indices in these models have been regressed onto low pass filtered SSTs, precipitation, sea level pressure and 200hPa zonal wind. The models are CESM2, HadGEM3-GC31-LL, MCM-UA-1-0, MIROC6, EC-Earth3-Veg, GISS-E2-1-G, CanESM5. Warm SST anomalies over the Indian Ocean are associated with positive rainfall anomalies (figure 10d) and low level convergence (figure 10g), implying that the SSTs are forcing the atmosphere rather than the atmosphere forcing the SSTs. Similar to figure 9g), a subtropical high is present, with positive 200hPa wind anomalies over China at 30-40N, though the wind anomalies extend further eastwards over the Pacific than in the atmosphere-only simulations (figures 10j and 9j).

Evidence for the second hypothesis, that the variance of EASJ variability explained by the Indian Ocean teleconnection is small, is provided by a comparison with the tropical Pacific index (figure 10b,e,h,k). Variations in the tropical Pacific index are linked to much larger SST anomalies over the Pacific than variations in the Indian Ocean index are over the Indian Ocean (figure 10a,b). Consequently, tropical Pacific circulation anomalies are of a much greater magnitude, for instance the magnitude of the 200hPa zonal wind anomaly is roughly double the equivalent for the Indian Ocean (figure 10j,k). Tropical Pacific anomalies are also much larger than those associated with the tropical Atlantic (figure 10c,f,i,l). Note that warm tropical Atlantic SSTs are associated with positive rainfall anomalies and a similar modulation of the sea level pressure patterns over the Atlantic and Pacific as in figure 9i). It therefore appears that while warm SST anomalies over the tropical Indian and Atlantic Oceans do result in a southward jet shift, the greater magnitude of decadal SST variability over the tropical Pacific means that this latter region explains by far the largest amount of EASJ variability. Unlike the piControl experiments, the magnitude of SST variability per area is constant by construction in the atmosphere-only runs, hence the Atlantic and Indian Ocean SSTs can have a larger influence.

To further underline the difference in inter-basin SST variability, we plot interannual vs decadal SST variability for each model for the Indian Ocean, tropical Pacific and tropical Atlantic regions in figure 11. In each case the SSTs at each grid-point have been linearly detrended to remove the influence of drift (in the case of the piControl models) or global warming (in observations) before calculating the mean over the region and the standard deviation. The grey box in figure 11b) shows the bounds of the Indian Ocean and tropical Atlantic scatter plots (figure 11a,c) indicating that tropical Pacific varibility is much larger on both timescales than for either of the other two regions in

the piControl models. The lack of external forcing in the piControl runs means that the piControl runs and observations are not directly comparable, however it is worth noting that decadal SST variability in the tropical Atlantic is higher in observations (black star) than in all but one piControl run (figure 11c). This means that the influence of the tropical Atlantic may be greater in reality than in the piControl runs and hence the Pacific may play a less dominant role. On the other hand, the magnitude of SST variability on both timescales is similar between observations and the piControl runs for the Indian Ocean and tropical Pacific (figure 11a,b).

6 | EXPLAINING INTER-MODEL DIFFERENCES

The correlation maps of EASJ EOF 1 with SST shown in figure 3 indicate that some models are much more strongly correlated with tropical SSTs than others. It is possible that the climatological state influences this teleconnection. For instance, differences in mean zonal wind could make the propagation of Rossby waves more or less favourable in some models. We investigate this by first defining a teleconnectivity index between tropical SSTs and the EASJ EOF 1. We do this by taking the mean correlation coefficient from the SST correlation maps on the left hand side of figure 3 for each model, within the latitudes 10S-10N (the index is insensitive to reasonable variations of these latitudes). The index is then multiplied by −1 so that a more positive teleconnectivity index implies a stronger tropical SST-EASJ teleconnection. Figure 12 shows correlation of this index with the climatology of each model. Neither the climatological mean 200hPa zonal wind, nor the mean SST appear to explain inter-model differences in teleconnectivity (figure 12a,b), however, mean precipitation is higher in the tropical Pacific region in models with greater teleconnectivity (figure 12c). This might be indicative that models with a larger magnitude of tropical Pacific variability have greater teleconnectivity. To specifically show the connection with decadal SST variability, we plot grid-point correlations of the teleconnectivity index with the standard deviation of low pass filtered SST. This confirms that the teleconnectivity index is positively correlated with SST variability in the tropical Pacific region. This is intuitive as larger decadal SST variability will provide larger anomalies to force an atmospheric circulation response and thus affect the EASJ. Interestingly, the teleconnectivity index is also negatively correlated with extratropical SST variability, particularly over the North Atlantic. That is, enhanced SST variability over the North Atlantic is linked to an EASJ which is less predictable based on tropical SSTs. Several studies have linked Atlantic Multidecadal Variability (AMV) to East Asian climate in both observations [53, 54, 55] and models [56, 57, 58] via modulation of the Circumglobal Teleconnection pattern (CGT), a wave train across Eurasia. It is possible that larger AMV in some models dominates decadal EASJ variability over tropical Pacific SSTs. However, many models do not capture the Atlantic SST-CGT teleconnection well [56]. This is also the case in the atmosphere-only simulations as SST forcing of the EASJ from the North Atlantic region, outside of 10S to 10N, is not a feature of the sensitivity map (figure 5a), hence this particular mechanism would not have been picked up in our analysis.

7 | DISCUSSION AND CONCLUSIONS

The aim of this study was to understand the extent to which SST variability modulates the East Asian summer jet (EASJ) on a decadal timescale. We have shown that EASJ variability is primarily characterised by a meridional shifting of the jet (figure 1c,e) and that a poleward shift of the jet is generally correlated with cool SSTs over most of the tropics in CMIP6 preindustrial control runs (piControl, figure 3a). A set of atmosphere-only model experiments forced with random SST patterns also showed a similar sensitivity of the EASJ to tropical SSTs (figure 5a). Although the atmosphere-only simulations are idealised, our analysis showed that the SST-EASJ teleconnection mechanisms were

similar between the atmosphere-only model and coupled piControl runs (figures 9 and 10). This suggests that tropical SSTs do force the jet response in coupled simulations.

Subsequently, we attempted to reconstruct EASJ variability in observations and in the piControl runs by projecting decadal SST anomalies onto the SST-sensitivity pattern calculated from the atmosphere-only simulations. Whilst, the decadal EASJ time series in the observational record has few degrees of freedom, the SST-based EASJ reconstruction did reproduce observed decadal jet variability well (figure 6b). The reconstruction also showed skill on interannual timescales (figure 6a), for which the observed time series has many degrees of freedom, hence this serves as validation of the jet reconstruction method.

Regarding the piControl runs, almost all models produced a reconstructed jet which was statistically significantly correlated with the true EASJ EOF 1 variability (figure 8a). The median model had a correlation coefficient of 0.43 and even if only the tropics were considered, most models still showed significant skill. Breaking the reconstruction skill down by region, the Pacific provided the most skill, however the tropical Atlantic also showed some significant skill. Considering the differences in skill coming from different regions, it appears that the magnitude of SST variability on decadal timescales explains much of the difference (figure 11). That is, tropical Pacific decadal SST variability is considerably larger than tropical Indian and Atlantic Ocean variability, hence the Pacific generates a larger atmospheric response, and thus explains the largest proportion of skill (figure 10a,b,c). However, we also noted that the piControl runs show weaker SST variability over the tropical North Atlantic than in observations (figure 11c). It is therefore possible that the tropical North Atlantic might play a larger role in the real Earth system, though the fact that this region did not contribute strongly to the SST-based EASJ reconstruction using observations suggests otherwise (figure 6c).

The strength of the tropical SST to EASJ teleconnection was shown to vary considerably between different models (figure 3). This was also explained by differences in the magnitude of decadal SST variability as models with strong teleconnectivity exhibited greater tropical Pacific SST variability (figure 12d). Intriguingly, models with a greater tropical SST teleconnectivity tended to have weaker North Atlantic SST variability. This suggests that Atlantic multidecadal variability may provide a competing influence on the EASJ. It would be interesting to investigate whether historical CMIP6 simulations show a similar result and to understand the underlying mechanism.

Finally, this work has shown that given accurate forecasts of multi-year variations in SST patterns, the EASJ may also be predictable on multi-year timescales. It would therefore be of interest to test whether there is sufficient skill in the SSTs of decadal hindcasts, for instance in the CMIP6 decadal climate prediction project [59], to make such EASJ forecasts.

acknowledgements

conflict of interest

The authors declare no conflict of interest.

references

[1] Wang H. The weakening of the Asian monsoon circulation after the end of 1970's. Advances in Atmospheric Sciences 2001 may;18(3):376–386. `https://link.springer.com/article/10.1007/BF02919316`.

[2] Wang B, Ding Q. Changes in global monsoon precipitation over the past 56 years. Geophysical Research Letters 2006 mar;33(6):L06711. `http://doi.wiley.com/10.1029/2005GL025347`.

[3] Wang Y, Chen X, Yan F. Spatial and temporal variations of annual precipitation during 1960-2010 in China. Quaternary International 2015 sep;380-381:5–13.

[4] Yu R, Wang B, Zhou T. Tropospheric cooling and summer monsoon weakening trend over East Asia. Geophysical Research Letters 2004 nov;31(22):1–4. `http://doi.wiley.com/10.1029/2004GL021270`.

[5] Gong DY, Ho CH. Shift in the summer rainfall over the Yangtze River valley in the late 1970s. Geophysical Research Letters 2002 may;29(10):78–1–78–4. `http://doi.wiley.com/10.1029/2001GL014523`.

[6] Ding Y, Wang Z, Sun Y. Inter-decadal variation of the summer precipitation in East China and its association with decreasing Asian summer monsoon. Part I: Observed evidences. International Journal of Climatology 2008 jul;28(9):1139–1161. `http://doi.wiley.com/10.1002/joc.1615`.

[7] Lei Y, Hoskins B, Slingo J. Exploring the interplay between natural decadal variability and anthropogenic climate change in summer rainfall over China. Part I: Observational evidence. Journal of Climate 2011 sep;24(17):4584–4599. `https://journals.ametsoc.org/view/journals/clim/24/17/2010jcli3794.1.xml`.

[8] Li H, Dai A, Zhou T, Lu J. Responses of East Asian summer monsoon to historical SST and atmospheric forcing during 1950-2000. Climate Dynamics 2010 mar;34(4):501–514. `https://link.springer.com/article/10.1007/s00382-008-0482-7`.

[9] Dong B, Sutton RT, Chen W, Liu X, Lu R, Sun Y. Abrupt summer warming and changes in temperature extremes over Northeast Asia since the mid-1990s: Drivers and physical processes. Advances in Atmospheric Sciences 2016 sep;33(9):1005–1023. `https://link.springer.com/article/10.1007/s00376-016-5247-3`.

[10] Qian Y, Leung LR, Ghan SJ, Giorgi F. Regional climate effects of aerosols over China: modeling and observation. Tellus B: Chemical and Physical Meteorology 2003 dec;55(4):914–934. `https://www.tandfonline.com/action/journalInformation?journalCode=zelb20`.

[11] Xu M, Chang CP, Fu C, Qi Y, Robock A, Robinson D, et al. Steady decline of east Asian monsoon winds, 1969–2000: Evidence from direct ground measurements of wind speed. Journal of Geophysical Research 2006 dec;111(D24):D24111. `http://doi.wiley.com/10.1029/2006JD007337`.

[12] He B, Bao Q, Li J, Wu G, Liu Y, Wang X, et al. Influences of external forcing changes on the summer cooling trend over East Asia. Climatic Change 2013 apr;117(4):829–841. `https://link.springer.com/article/10.1007/s10584-012-0592-4`.

[13] Song F, Zhou T, Qian Y. Responses of East Asian summer monsoon to natural and anthropogenic forcings in the 17 latest CMIP5 models. Geophysical Research Letters 2014 jan;41(2):596–603. `http://doi.wiley.com/10.1002/2013GL058705`.

[14] Wang T, Wang HJ, Otterå OH, Gao YQ, Suo LL, Furevik T, et al. Anthropogenic agent implicated as a prime driver of shift in precipitation in eastern China in the late 1970s. Atmospheric Chemistry and Physics 2013 dec;13(24):12433–12450.

[15] Ueda H, Iwai A, Kuwako K, Hori ME. Impact of anthropogenic forcing on the Asian summer monsoon as simulated by eight GCMs. Geophysical Research Letters 2006 mar;33(6):L06703. `http://doi.wiley.com/10.1029/2005GL025336`.

[16] Zhu C, Wang B, Qian W, Zhang B. Recent weakening of northern East Asian summer monsoon: A possible response to global warming. Geophysical Research Letters 2012 may;39(9):n/a–n/a. http://doi.wiley.com/10.1029/2012GL051155.

[17] Tian F, Dong B, Robson J, Sutton R. Forced decadal changes in the East Asian summer monsoon: the roles of greenhouse gases and anthropogenic aerosols. Climate Dynamics 2018 nov;51(9-10):3699–3715. https://doi.org/10.1007/s00382-018-4105-7.

[18] Jiang D, Wang H. Natural interdecadal weakening of East Asian summer monsoon in the late 20th century. Chinese Science Bulletin 2005 mar;50(17):1923–1929. http://cera-www.dkrz.de/IPCC{_}DDC/index.html.

[19] Lei Y, Hoskins B, Slingo J. Natural variability of summer rainfall over China in HadCM3. Climate Dynamics 2014 jan;42(1-2):417–432. https://link.springer.com/article/10.1007/s00382-013-1726-8.

[20] Liang XZ, Wang WC. Associations between China monsoon rainfall and tropospheric jets. Quarterly Journal of the Royal Meteorological Society 1998 oct;124(552):2597–2623. http://doi.wiley.com/10.1002/qj.49712455204.

[21] Lu R. Associations among the Components of the East Asian Summer Monsoon System in the Meridional Direction. Journal of the Meteorological Society of Japan 2004 feb;82(1):155–165. http://joi.jlc.jst.go.jp/JST.JSTAGE/jmsj/82.155?from=CrossRef.

[22] Lin Z, Lu R. Interannual meridional displacement of the East Asian upper-tropospheric jet stream in summer. Advances in Atmospheric Sciences 2005;22(2):199–211. https://link.springer.com/article/10.1007/BF02918509.

[23] Huang DQ, Zhu J, Zhang YC, Huang AN. The different configurations of the East Asian polar front jet and subtropical jet and the associated rainfall anomalies over eastern China in summer. Journal of Climate 2014 nov;27(21):8205–8220. http://ncc.cma.gov.cn.

[24] Xie Z, Du Y, Yang S. Zonal extension and retraction of the subtropical westerly jet stream and evolution of precipitation over East Asia and the Western Pacific. Journal of Climate 2015 sep;28(17):6783–6798. http://www.esrl.noaa.gov/psd/data/gridded/data.

[25] Ren Y, Zhou B, Song L, Xiao Y. Interannual variability of western North Pacific subtropical high, East Asian jet and East Asian summer precipitation: CMIP5 simulation and projection. Quaternary International 2017 jun;440:64–70.

[26] Lin Z, Fu Y, Lu R. Intermodel Diversity in the Zonal Location of the Climatological East Asian Westerly Jet Core in Summer and Association with Rainfall over East Asia in CMIP5 Models. Advances in Atmospheric Sciences 2019 jun;36(6):614–622. https://doi.org/10.1007/s00376-019-8221-z.

[27] Yan Y, Li C, Lu R. Meridional Displacement of the East Asian Upper-tropospheric Westerly Jet and Its Relationship with the East Asian Summer Rainfall in CMIP5 Simulations. Advances in Atmospheric Sciences 2019 nov;36(11):1203–1216. https://doi.org/10.1007/s00376-019-9066-1.

[28] Qu X, Huang G. Impacts of tropical Indian Ocean SST on the meridional displacement of East Asian jet in boreal summer. International Journal of Climatology 2012 nov;32(13):2073–2080. http://doi.wiley.com/10.1002/joc.2378.

[29] Lin XZ, Li CF, Lin ZD, Lu RY. Close relationship between the East Asian westerly jet and Russian far East surface air temperature in summer. Atmospheric and Oceanic Science Letters 2018 may;11(3):282–286. https://www.tandfonline.com/doi/full/10.1080/16742834.2018.1467726.

[30] Xie SP, Hu K, Hafner J, Tokinaga H, Du Y, Huang G, et al. Indian Ocean capacitor effect on Indo-Western pacific climate during the summer following El Niño. Journal of Climate 2009 feb;22(3):730–747. https://journals.ametsoc.org/view/journals/clim/22/3/2008jcli2544.1.xml.

[31] Lei Y. Potential Correlation between the Decadal East Asian Summer Monsoon Variability and the Pacific Decadal Oscillation. Atmospheric and Oceanic Science Letters 2013 jan;6(5):394–397. https://www.tandfonline.com/action/journalInformation?journalCode=taos20.

[32] Zhang Z, Sun X, Yang XQ.   Understanding the interdecadal variability of East Asian summer monsoon precipita-
tion: Joint influence of three oceanic signals.   Journal of Climate 2018 jul;31(14):5485–5506.   `www.ametsoc.org/`
`PUBSReuseLicenses`.

[33] Eyring V, Bony S, Meehl GA, Senior CA, Stevens B, Stouffer RJ, et al. Overview of the Coupled Model Intercomparison
Project Phase 6 (CMIP6) experimental design and organization. Geoscientific Model Development 2016 may;9(5):1937–
1958.

[34] Baker HS, Woollings T, Forest CE, Allen MR. The linear sensitivity of the north atlantic oscillation and eddy-driven jet
to SSTs. Journal of Climate 2019 oct;32(19):6491–6511. `https://doi.org/10.1175/JCLI-D-19-`.

[35] Li W, Forest CE, Barsugli J. Comparing two methods to estimate the sensitivity of regional climate simulations to tropical
SST anomalies. Journal of Geophysical Research: Atmospheres 2012 oct;117(D20):20103. `http://doi.wiley.com/10.`
`1029/2011JD017186`.

[36] Li W, Forest CE. Estimating the sensitivity of the atmospheric teleconnection patterns to SST anomalies using a linear
statistical method. Journal of Climate 2014 dec;27(24):9065–9081. `https://journals.ametsoc.org/view/journals/`
`clim/27/24/jcli-d-14-00231.1.xml`.

[37] Titchner HA, Rayner NA. The Met Office Hadley Centre sea ice and sea surface temperature data set, version 2: 1. Sea
ice concentrations. Journal of Geophysical Research: Atmospheres 2014 mar;119(6):2864–2889. `http://doi.wiley.`
`com/10.1002/2013JD020316`.

[38] Poli P, Hersbach H, Dee DP, Berrisford P, Simmons AJ, Vitart F, et al. ERA-20C: An atmospheric reanalysis of the twentieth
century. Journal of Climate 2016 jun;29(11):4083–4097. `http://apps.ecmwf.int`.

[39] Kobayashi S, Ota Y, Harada Y, Ebita A, Moriya M, Onoda H, et al. The JRA-55 Reanalysis: General Specifications and
Basic Characteristics. Journal of the Meteorological Society of Japan Ser II 2015 mar;93(1):5–48. `https://www.jstage.`
`jst.go.jp/article/jmsj/93/1/93{\_}2015-001/{\_}article`.

[40] Kalnay E, Kanamitsu M, Kistler R, Collins W, Deaven D, Gandin L, et al. The NCEP/NCAR 40-year reanalysis project.
Bull Am Meteorol Soc 1996;77(3):437–471.

[41] Dawson A. eofs: A Library for EOF Analysis of Meteorological, Oceanographic, and Climate Data. Journal of Open
Research Software 2016 apr;4(1):14. `http://openresearchsoftware.metajnl.com/articles/10.5334/jors.122/`.

[42] Barsugli JJ, Battisti DS. The basic effects of atmosphere-ocean thermal coupling on midlatitude variability. Journal of
the Atmospheric Sciences 1998 feb;55(4):477–493. `https://journals.ametsoc.org/view/journals/atsc/55/4/1520-`
`0469{\_}1998{\_}055{\_}0477{\_}tbeoao{\_}2.0.co{\_}2.xml`.

[43] Barsugli J, Sardeshmukh P. Global Atmospheric Sensitivity to Tropical SST Anomalies throughout the Indo-Pacific
Basin. Journal of Climate 2002;15(23):3427–3442. `https://journals.ametsoc.org/view/journals/clim/15/23/1520-`
`0442{\_}2002{\_}015{\_}3427{\_}gastts{\_}2.0.co{\_}2.xml`.

[44] Ebisuzaki W. A method to estimate the statistical significance of a correlation when the data are serially correlated. Jour-
nal of Climate 1997 sep;10(9):2147–2153. `https://journals.ametsoc.org/view/journals/clim/10/9/1520-0442{\_`
`}1997{\_}010{\_}2147{\_}amtets{\_}2.0.co{\_}2.xml`.

[45] North GR, Bell TL, Cahalan RF, Moeng FJ. Sampling Errors in the Estimation of Empirical Orthogonal Functions. Monthly
Weather Review 1982 jul;110(7):699–706. `https://journals.ametsoc.org/view/journals/mwre/110/7/1520-0493{\_`
`}1982{\_}110{\_}0699{\_}seiteo{\_}2{\_}0{\_}co{\_}2.xml`.

[46] Newman M, Alexander MA, Ault TR, Cobb KM, Deser C, Di Lorenzo E, et al. The Pacific decadal oscillation, revisited.
Journal of Climate 2016 jun;29(12):4399–4427. `https://journals.ametsoc.org/view/journals/clim/29/12/jcli-d-`
`15-0508.1.xml`.

[47] Wu B, Zhou T, Li T. Contrast of rainfall-SST relationships in the western North Pacific between the ENSO-developing and ENSO-decaying summers. Journal of Climate 2009 aug;22(16):4398–4405. `www.cpc.ncep.noaa.gov/products/analysis{\_}monitoring/`.

[48] Wu B, Zhou T, Li T. Seasonally evolving dominant interannual variability modes of East Asian climate. Journal of Climate 2009 jun;22(11):2992–3005. `https://journals.ametsoc.org/view/journals/clim/22/11/2008jcli2710.1.xml`.

[49] Seager R, Harnik N, Kushnir Y, Robinson W, Miller J. Mechanisms of Hemispherically Symmetric Climate Variability in: Journal of Climate Volume 16 Issue 18 (2003). Journal of Climate 2003;16(18):2960–2978. `https://journals.ametsoc.org/view/journals/clim/16/18/1520-0442{\_}2003{\_}016{\_}2960{\_}mohscv{\_}2.0.co{\_}2.xml`.

[50] Lu J, Chen G, Frierson DMWWW. Response of the zonal mean atmospheric circulation to El Niño versus global warming. Journal of Climate 2008;21(22):5835–5851.

[51] Rong XY, Zhang RH, Li T. Impacts of Atlantic sea surface temperature anomalies on Indo-East Asian summer monsoon-ENSO relationship. Chinese Science Bulletin 2010 aug;55(22):2458–2468. `www.springerlink.com`.

[52] Hoskins BJ, Karoly DJ. The Steady Linear Response of a Spherical Atmosphere to Thermal and Orographic Forcing. Journal of the Atmospheric Sciences 1981;38(6):1179–1196.

[53] Ding Q, Wang B. Circumglobal teleconnection in the Northern Hemisphere summer. Journal of Climate 2005 sep;18(17):3483–3505. `https://journals.ametsoc.org/view/journals/clim/18/17/jcli3473.1.xml`.

[54] Wu B, Zhou T, Li T. Impacts of the Pacific-Japan and circumglobal teleconnection patterns on the interdecadal variability of the east Asian summer monsoon. Journal of Climate 2016 may;29(9):3253–3271. `http://dx.doi.org/10.1175/JCLI-D-15-`.

[55] Hong X, Lu R, Li S. Amplified summer warming in Europe-West Asia and Northeast Asia after the mid-1990s. Environmental Research Letters 2017 sep;12(9):094007. `https://doi.org/10.1088/1748-9326/aa7909`.

[56] Lin JS, Wu B, Zhou TJ. Is the interdecadal circumglobal teleconnection pattern excited by the Atlantic multidecadal Oscillation? Atmospheric and Oceanic Science Letters 2016 nov;9(6):451–457. `https://www.tandfonline.com/doi/full/10.1080/16742834.2016.1233800`.

[57] Monerie PA, Robson J, Dong B, Dunstone N. A role of the Atlantic Ocean in predicting summer surface air temperature over North East Asia? Climate Dynamics 2018 jul;51(1-2):473–491. `https://link.springer.com/article/10.1007/s00382-017-3935-z`.

[58] Monerie PA, Robson J, Dong B, Hodson D. Role of the Atlantic multidecadal variability in modulating East Asian climate. Climate Dynamics 2021 jan;56(1-2):381–398. `https://doi.org/10.1007/s00382-020-05477-y`.

[59] Boer GJ, Smith DM, Cassou C, Doblas-Reyes F, Danabasoglu G, Kirtman B, et al. The Decadal Climate Prediction Project (DCPP) contribution to CMIP6. Geoscientific Model Development 2016 oct;9(10):3751–3777.

GRAPHICAL ABSTRACT
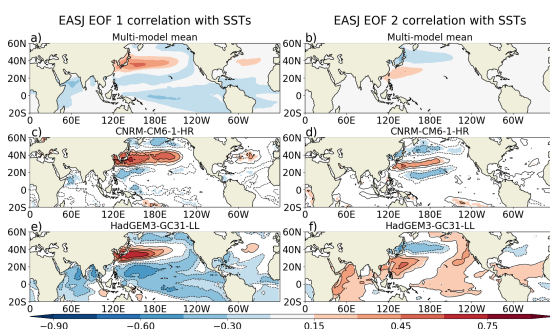
The East Asian summer jet (EASJ) modulates monsoon rainfall over eastern China and has been shown to vary on multi-year timescales. However, the drivers of this multi-year variability have not been investigated. In this study, we investigate the extent to which sea surface temperature (SST) variability modulates the EASJ

using an ensemble of climate model simulations. In particular, we show that SST variability over the tropical Pacific is a strong driver of jet variations on multi-year timescales.
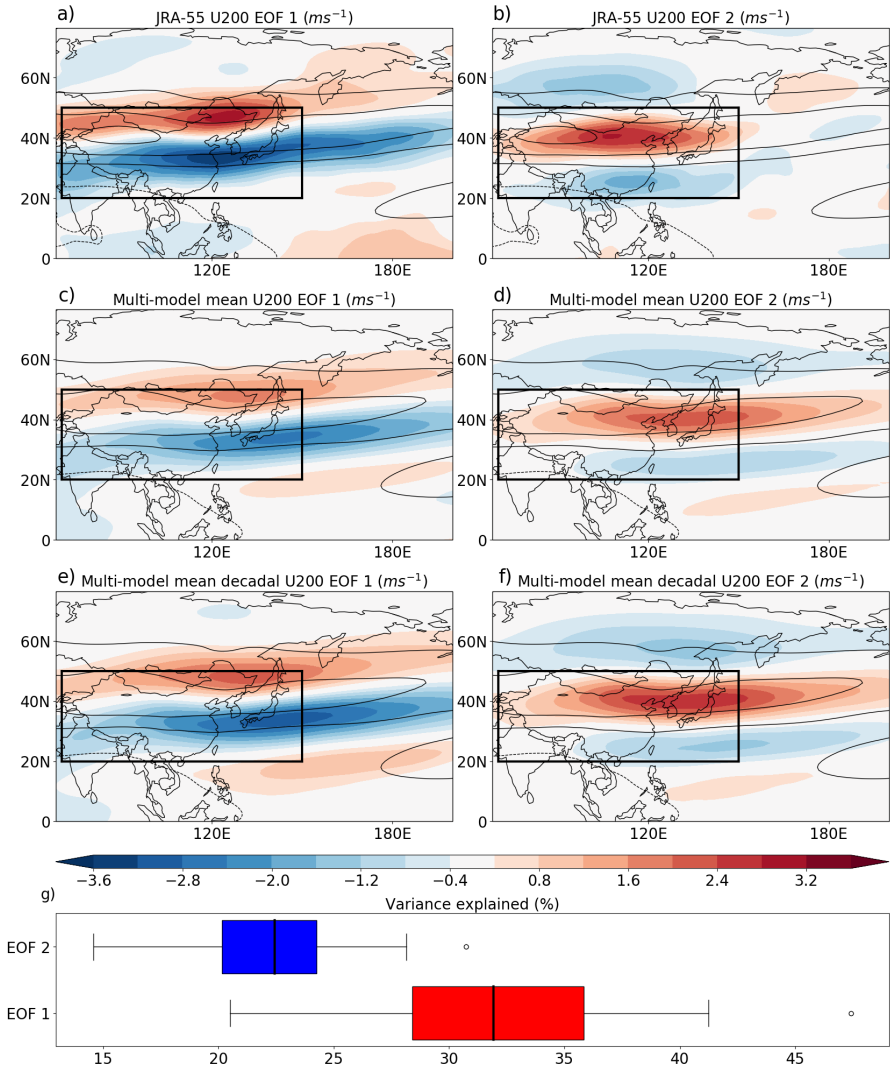
FIGURE 1 The two EASJ EOF indices regressed onto 200hPa zonal wind for the summer (JJA) season. This is shown by colours for a,b) interannual JRA-55 data and c,d) the multi-model mean of the regression maps for all 28 CMIP6 models using interannual data. e,f) is the same as c,d) except a 7 year running mean has been applied to the EASJ EOF indices after calculating the EOFs to extract the decadal signal, and this has been regressed onto zonal wind data which has also been low pass filtered at each grid-point. Unfilled, black contours indicate the zonal wind climatology in a-f), contoured every $10ms^{-1}$. Finally, g) shows box plots of the variance explained by EOFs 1 and 2.
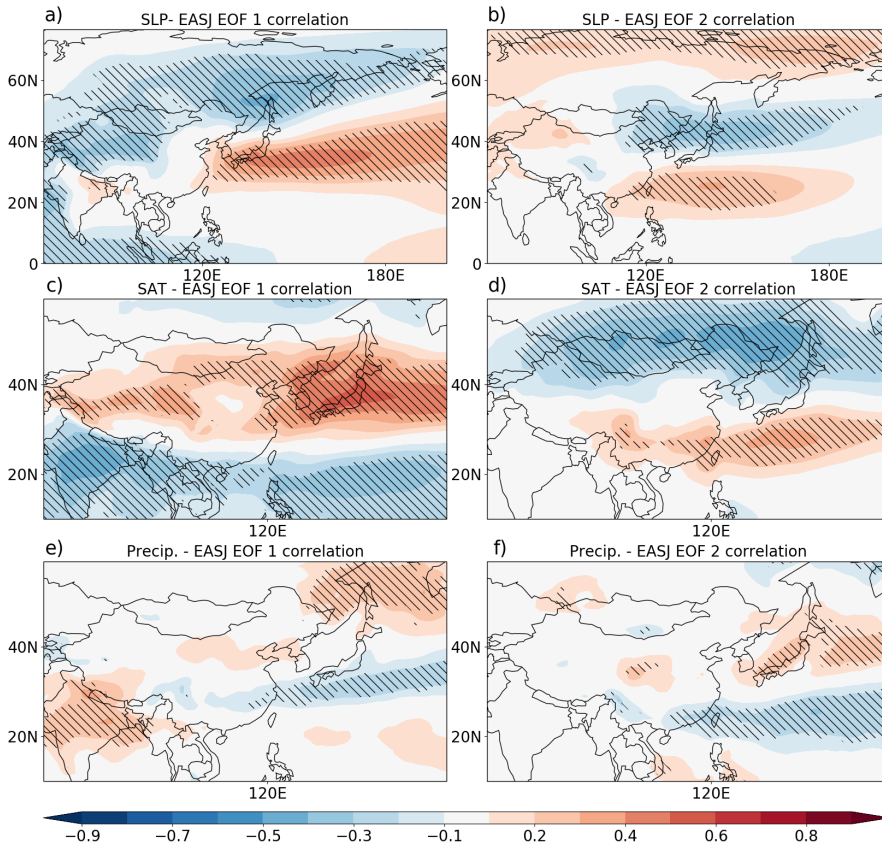
FIGURE 2 Multi-model means (28 models) of correlation maps of EASJ EOF indices with surface climate variables. In each case, both the EASJ EOF indices and surface climate variables have been low pass filtered with a 7 year running mean to extract the decadal signal. The maps show the principal component time series associated with a,c,e) EOF 1 and b,d,f) EOF 2, correlated with a,b) sea level pressure, c,d) surface air temperature and e,f) precipitation for the summer (JJA) season. In each panel, colours indicate the multi-model mean correlation and hatching indicates where at least 80% of models agree on the sign of the correlation coefficient at that grid-point.
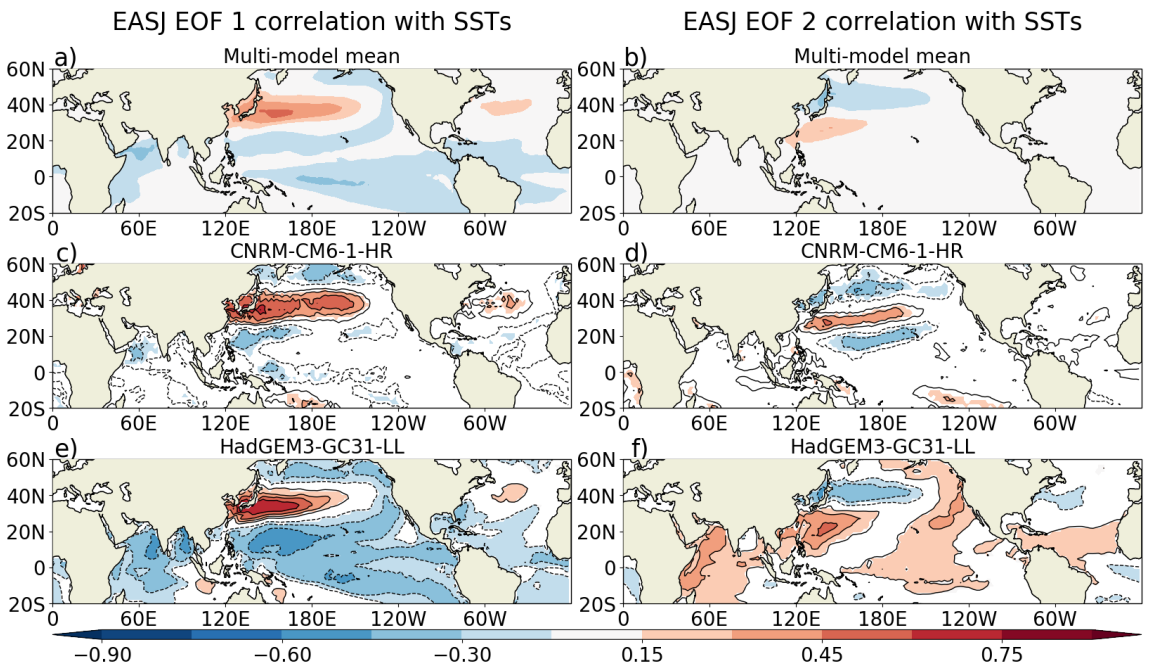
FIGURE 3 Maps showing correlations between the EASJ EOF indices and low-pass filtered SSTs at each grid-point for JJA. The multi-model mean SST correlation values are shown in a) and b), with correlations for the models CNRM-CM6-1-HR and HadGEM3-GC31-LL shown in c,d) and e,f) respectively. These two individual models are plotted to represent the fact that tropical SSTs are weakly correlated with EASJ variability in some models (e.g. CNRM-CM6-1-HR), but strongly correlated with the jet in others (e.g. HadGEM3-GC31-LL). In panels c-f), unfilled contours are drawn every 0.15, excluding the zero contour, with colours shown where values are significant at the 95% level.
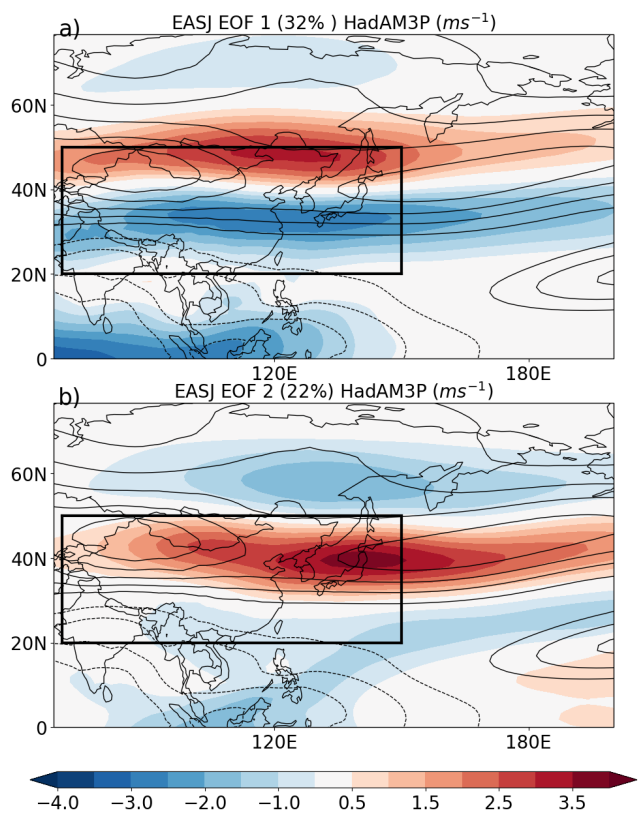
FIGURE 4 Maps showing regressions of 200hPa zonal wind onto the EASJ EOF indices calculated from the HadAM3P atmosphere-only model (colours) for JJA. Unfilled contours indicate the summertime zonal wind climatology, contoured every $5ms^{-1}$. A black box shows the East Asia region and the variance explained by each pattern is indicated by the percentages in brackets.
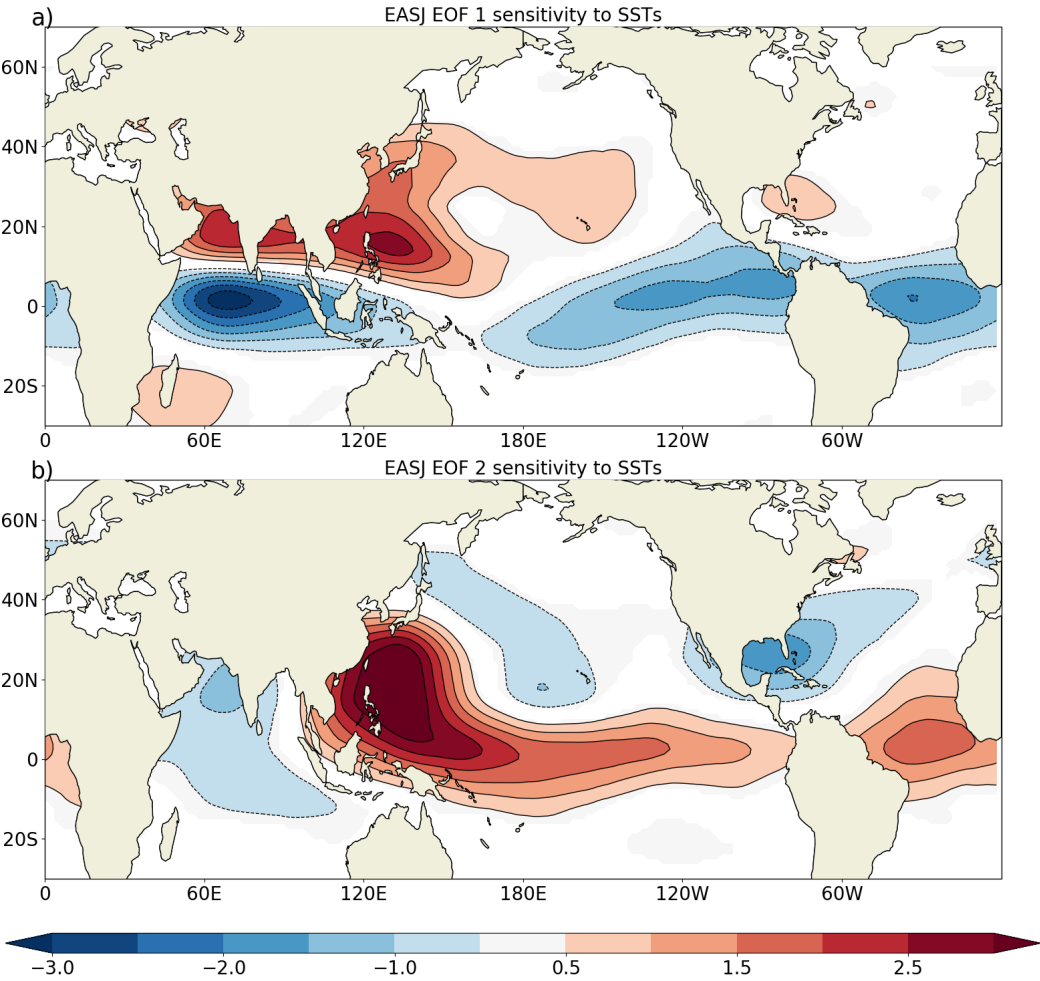
FIGURE 5 EASJ EOF sensitivity maps, showing the sensitivity of the jet EOF indices to SST perturbations at a given location during JJA. Colours show coefficients significant at the 95% level. The units are $\times 10^6 \, km^{-2} K^{-1}$.
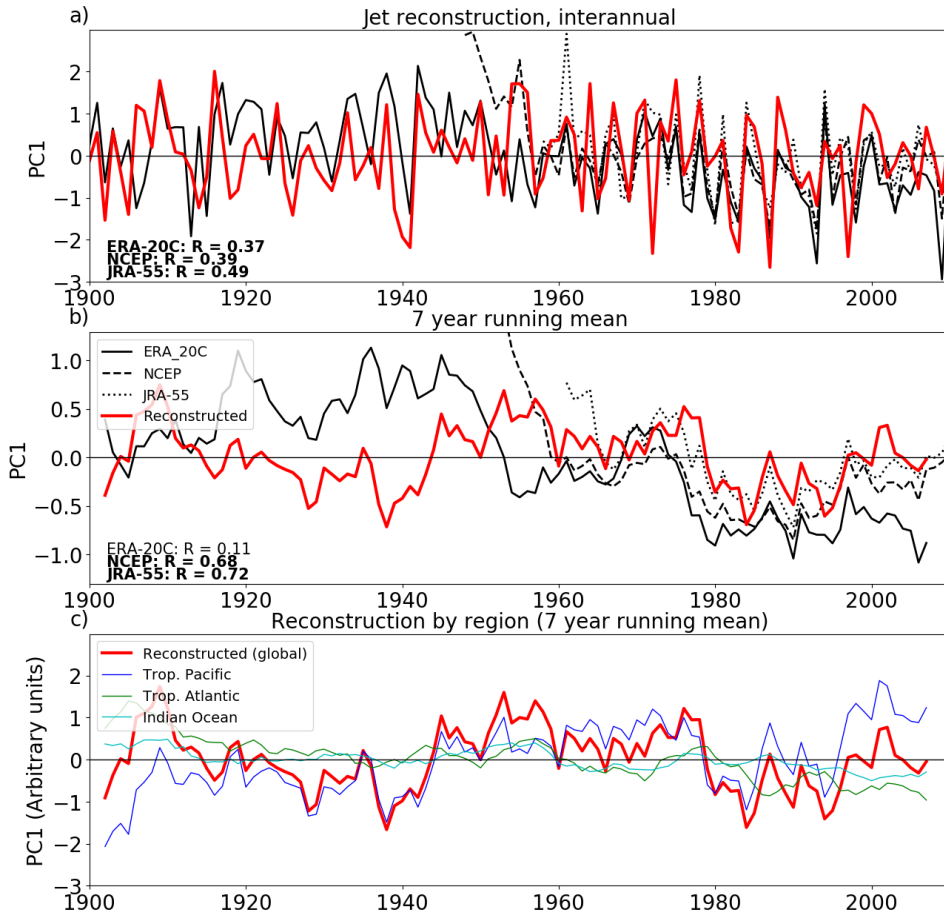
FIGURE 6 SST-based reconstructions of EASJ EOF 1 in comparison to EASJ EOF 1 calculated from three reanalysis datasets. In a), the interannual variability of the reconstruction is shown alongside ERA-20C, NCEP/NCAR and JRA-55. Correlation coefficients between the reconstruction and the EASJ EOF 1 indices from the three reanalyses are shown in the bottom right corner, with bold indicating statistical significance at the 95% level. In b), a 7 year running mean has been applied to the time series' in a) to show the decadal variability. In c), the low pass filtered jet reconstruction (red) is separated into contributions from the tropical Pacific (blue), tropical Atlantic (green) and Indian Ocean (cyan).
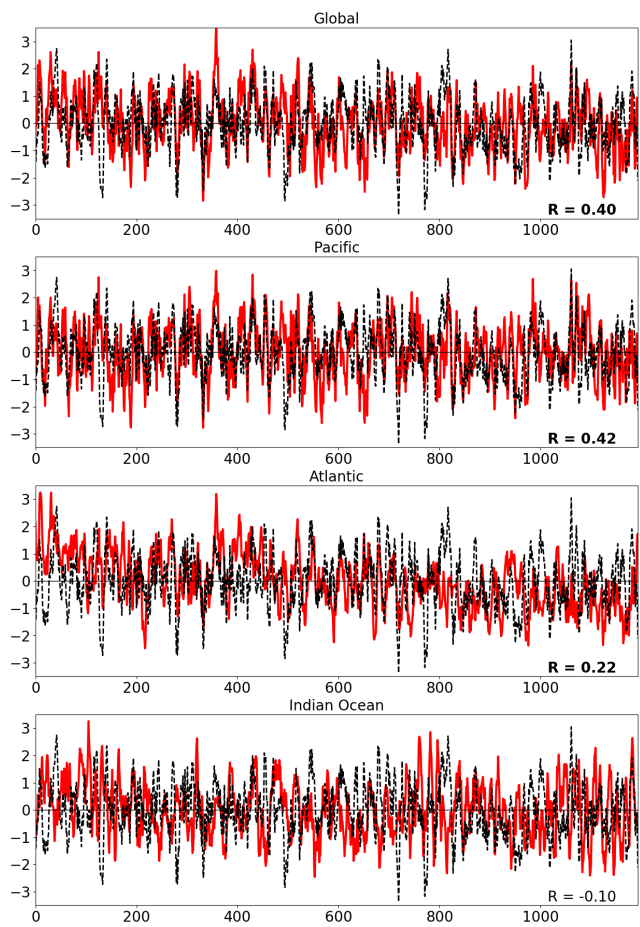
FIGURE 7 SST-based reconstructions of the EASJ EOF 1 in CESM2 (red) in comparison to the actual EASJ EOF 1 index (black, dashed). This is shown for SST anomaly projections onto a) the entire sensitivity pattern, b) the Pacific region, c) the Atlantic region and d) the Indian Ocean region. Correlation coefficients are shown in the bottom right with bold indicating statistical significance at the 95% level.
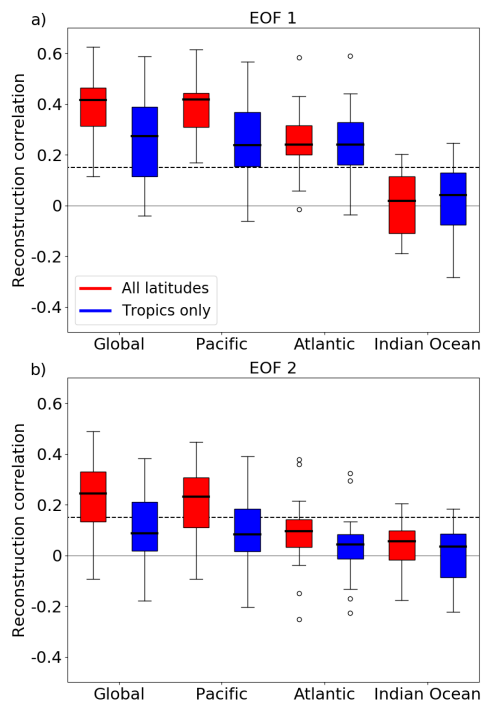
FIGURE 8 Box plots showing correlations between EASJ indices and SST-based reconstructions for all models for projections onto given regions and for a) EOF 1 and b) EOF 2. Red box plots show projections onto the entire sensitivity pattern, while blue box plots of EASJ reconstructions based only on projections onto the tropics. The 95% significance level for model simulations which last for 500 years is plotted as a dashed line.
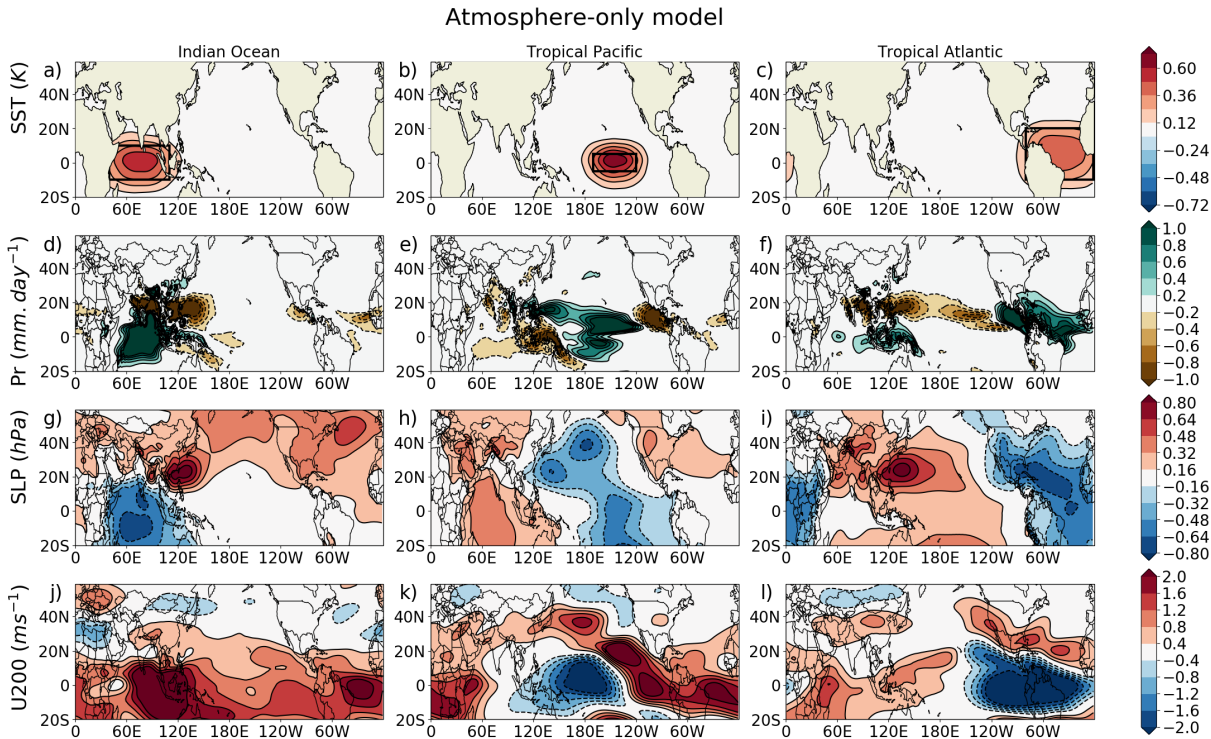
FIGURE 9 Regression of SST indices from the atmosphere-only runs onto a-c) SSTs (K), d-f) daily mean precipitation ($mm\,day^{-1}$), g-i) sea level pressure (hPa) and j-l) 200hPa zonal wind (ms^{-1}). All values shown by colours are significant at the 95% level. Black boxes in a-c) indicate the region which defines each SST index.
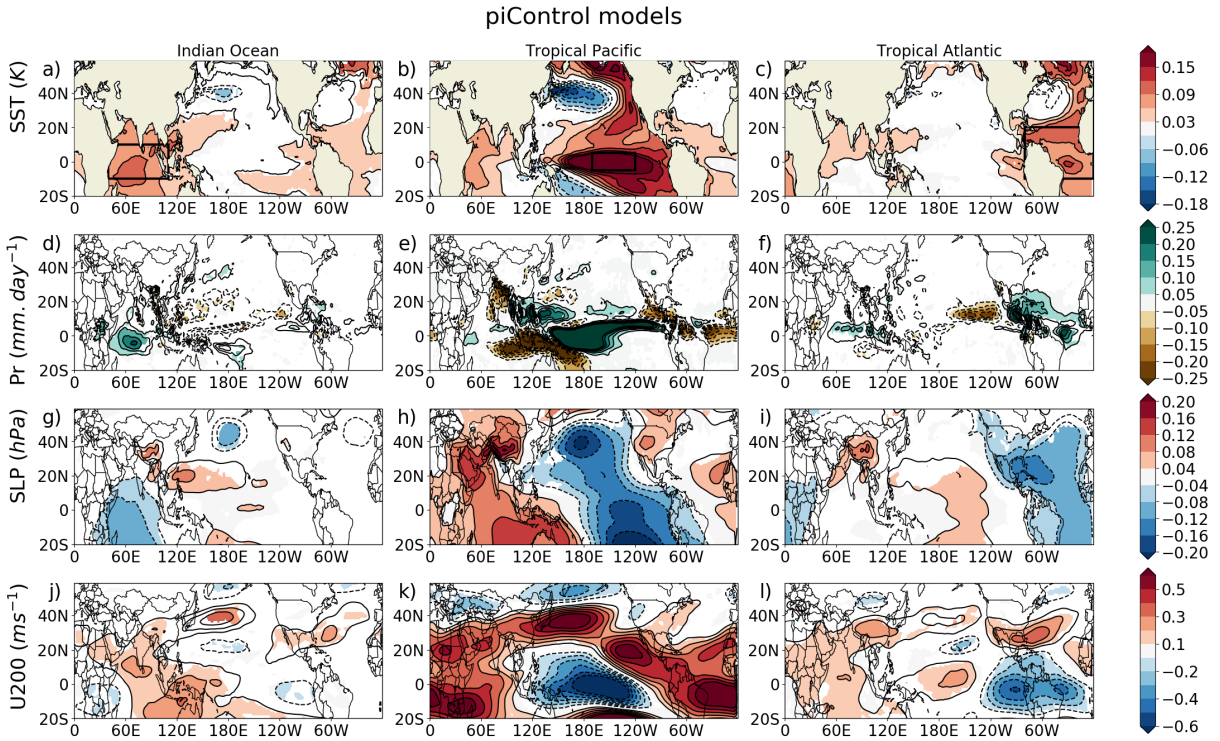
FIGURE 10 Composite regression maps of seven models with the strongest tropical SST-EASJ teleconnection strengths. The maps show the mean of these models for the regression of SST indices onto low pass filtered a-c) SST (K), d-f) precipitation ($mm\ day^{-1}$), g-i) sea level pressure (hPa) and j-l) 200hPa zonal wind (ms^{-1}). The tropical Pacific index has been regressed out of both the Indian Ocean and Atlantic Ocean indices. In a-c) black boxes indicate the region used to define the SST index.
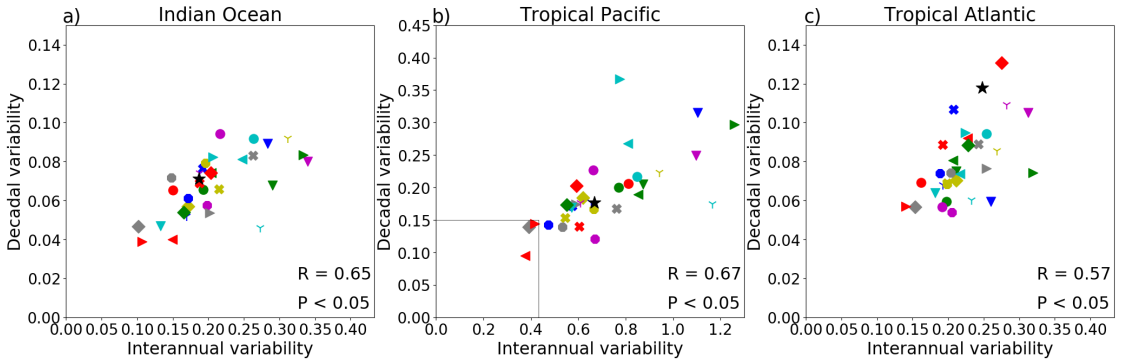
FIGURE 11 Decadal vs interannual SST variability in JJA for all piControl runs in the regions used for figures 8 and 9. The interannual variability is defined as the standard deviation of the mean SST in the given region and the decadal variability is the same, but with a 7 year running mean applied before calculating the standard deviation. Each symbol is a different CMIP6 model and the black star shows the value for HadISST. The regions shown are a) the Indian Ocean, b) tropical Pacific and c) tropical Atlantic. Note that the x and y axes are the same in a) and c), but different in b). The grey box in b) shows the bounds of scatter plots a) and c).
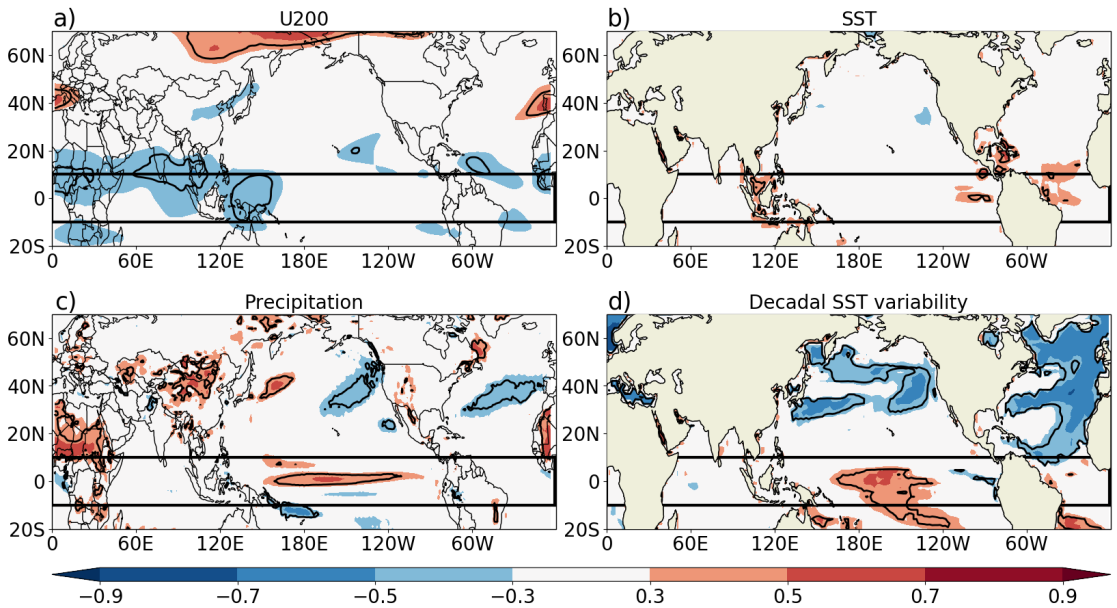

FIGURE 12 Correlation maps of the EASJ-SST teleconnectivity index (see text for details) with model climatology values, across all models, at each grid-point. The teleconnectivity index is correlated with a) 200hPa zonal wind climatology, b) SST climatology, c) precipitation climatology and d) the standard deviation of 7 year low pass filtered SST. A thick black contour indicates regions where correlations are significant at the 95% level. A black box shows the region over which the EASJ-SST teleconnectivity index is calculated.